In Vivo Probes

DOI: 10.1002/anie.201007461

Design of Highly Emissive Polymer Dot Bioconjugates for In Vivo Tumor Targeting**

*Changfeng Wu, Stacey J. Hansen, Qiong Hou, Jiangbo Yu, Maxwell Zeigler, Yuhui Jin, Daniel R. Burnham, Jason D. McNeill, James M. Olson, and Daniel T. Chiu**

Nanoparticle-based diagnostic and therapeutic agents have attracted considerable interest because of their potential for applications in clinical oncology and other biomedical research.[1] Versatile nanostructures for in vivo applications, such as lipid and polymeric nanocapsules for drug delivery,[2] iron oxide nanoparticles for magnetic resonance imaging,[3] gold nanoparticles for X-ray computed tomography,[4] and quantum dots (Qdots) for fluorescence imaging,[5] have been reported. Qdots represent one of the exciting nanotechnologies that have been translated to biology in the past decade. Their size-tunable luminescence makes them appealing as multicolor fluorophores for biological labelling, imaging, and sensing.[6,7] For in vivo applications, however, the intrinsic toxicity of Qdots is of critical concern,[8] which may impede their final clinical application. Therefore, the design of bright probes with biologically benign materials is highly desirable for many in vivo clinical purposes.

Semiconducting polymer dots (Pdots) represent a new class of fluorescent probes because of their exceptional brightness and their nontoxic features.[9–15] Although still at an early stage of development, Pdots attract intense interest.[12,13] Researchers have developed various methods to improve the versatility and functions of Pdots for biomedical studies, such as tuning the emission color,[16] exploring new preparation methods,[17] engineering the particle surface,[18] doping functional sensing molecules,[19,20] encapsulating magnetic materials,[21] and mapping the sentinel lymph node as a first in vivo study.[22] We have recently developed a general method to form Pdot–bioconjugates, and have demonstrated their applications in specific cellular targeting and bioorthogonal labeling.[23,24]

Despite various efforts, there are still several challenges associated with Pdots as in vivo probes. Firstly, the fluorescence brightness of Pdots in the red and near infrared (NIR) is generally limited by their low quantum yields. Secondly, it is unclear whether Pdot-based probes can be specifically delivered to diseased tissues in vivo. Herein we show highly fluorescent Pdots that consist of optimally tailored semiconducting polymer blends for in vivo tumor targeting. The polymer-blend dots (PBdots) exhibited large absorptivity (3.0×10^7 $cm^{-1}M^{-1}$ at 488 nm) and efficient deep-red emission (quantum yield = 0.56), thus making them approximately 15 times brighter than the commercial Qdots that emit at 655 nm. We covalently attacheded the PBdots to a tumor-specific peptide ligand, and demonstrated their specific targeting to malignant brain tumors in a genetically engineered mouse model.

Various semiconducting polymers can be used to prepare small Pdots as fluorescent labels.[11] Polyfluorenes (PF) and their derivatives in particular exhibit great flexibility for the design of fluorescent probes as shown by the significant progress made so far in tuning their emission color from blue to deep red by the introduction of narrow-band-gap monomers into the polymer backbone.[25,26] However, the fluorescence quantum yield, particularly in the deep-red region, precipitously drops as the concentration of the narrow-band-gap monomers is increased. As a trade-off, therefore, only a small amount of narrow-band-gap monomers can be incorporated into the PF copolymer so as to maintain a high fluorescence quantum yield. This constraint results in deep-red emitting Pdots that only have significant absorption features in the ultraviolet (UV) region (see Figure S1 in the Supporting Information), which is a severe drawback for in vivo applications. Herein we describe our strategy to overcome this issue by designing polymer-blended Pdots that have both excellent absorption cross-sections in the visible range and high quantum yields in deep-red emission.

Based on the efficient intra-particle energy transfer in Pdots,[19,27] we have designed nanoparticles that consist of donor–acceptor polymer blends to overcome the UV-absorption limitation. The polymer-blend dots (PBdots) were prepared by using a visible-light-harvesting polymer (PFBT) as the donor and an efficient deep-red emitting polymer (PFDBT5) as the acceptor (Figure 1a). Since the donor and acceptor polymers were closely packed into single dots, intra-

[*] C. Wu, M. Zeigler, Y. Jin, D. R. Burnham, Prof. D. T. Chiu
Department of Chemistry, University of Washington
Seattle, WA 98195 (USA)
Fax: (+1) 206-685-8665
E-mail: chiu@chem.washington.edu
S. J. Hansen, Prof. J. M. Olson
Clinical Research Division
Fred Hutchinson Cancer Research Centre, Seattle, WA 98109 (USA)
J. Yu, Prof. J. D. McNeill
Department of Chemistry, Clemson University
Clemson, SC 29634 (USA)
Prof. Q. Hou
School of Chemistry and Environment
South China Normal University, Guangzhou, Guangdong 510631 (China)

[**] This work was supported by the National Institutes of Health (CA147837 and NS062725 to D.T.C.; CA135491 and CA112350-03 to J.M.O.; GM 081040 to J.D.M.). We acknowledge support from the Keck Imaging Center, the Center of Nanotechnology at the University of Washington, and the Seattle Children's Research Institute Brain Tumor Endowment.

Supporting information for this article is available on the WWW under http://dx.doi.org/10.1002/anie.201007461.

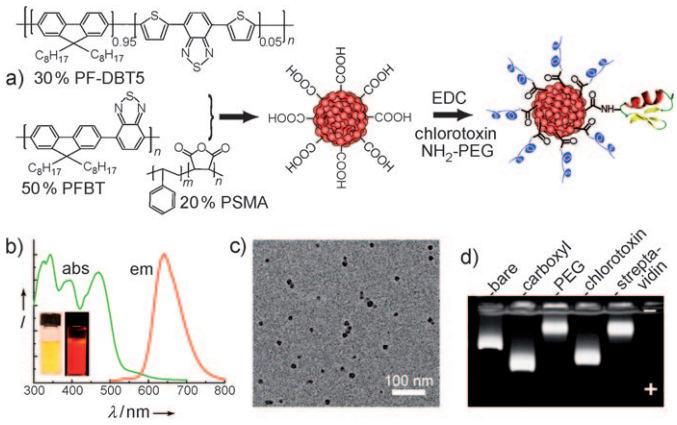

Figure 1. a) PBdot functionalization and CTX conjugation. A light-harvesting polymer PFBT, a red-emitting polymer PF-DBT5, and a functional polymer PSMA were cocondensed to form highly fluorescent PBdots with surface carboxyl groups. The carboxyl groups enabled further surface conjugation to a tumor-specific peptide ligand CTX (depicted as red-green-yellow string). b) Absorption and emission spectra of PBdot. Inset: photographs of an aqueous PBdot solution under illumination with ambient light (left) and UV light (right). c) TEM image of carboxyl-functionalized PBdots. d) Gel electrophoresis of functionalized and bioconjugated PBdots in a 0.7% agarose gel.

We performed single-particle imaging to compare the brightness of the PBdot against that of a Qdot that emits at 655 nm (the brightest commercially available Qdot probe from Invitrogen). We used 488 nm laser excitation power so that Qdot 655 could be reasonably detected (Figure 2a); under identical acquisition and laser conditions, however, the majority of PBdots actually saturated the detector. This prominent difference is attributed to the high molar extinction coefficient of PBdots (ca. $3.0\times10^7\ cm^{-1}M^{-1}$ at 488 nm for nanoparticles of approximately 15 nm diameter). To avoid detector saturation, we used a neutral density filter (optical density of 1, which blocks 90% of the emitted fluorescence) together with the emission filter to obtain single-particle fluorescence images of PBdots (Figure 2b). Fluorescence images of thousands of individual particles were collected and their fluorescence intensities were back-calculated according to the attenuation factor. Fluorescence intensity distribution indicated that PBdots were approximately 15 times brighter than Qdot 655 (Figure 2c), which is consistent with the brightness comparison based on the bulk spectra analysis. Fluorescence lifetime of PBdots was determined to be 3.5 ns with a time-correlated single-photon counting instrument (TCSPC; Figure S4).

particle energy transfer resulted in complete quenching of the PFBT donor and intense fluorescence from the acceptor polymer alone (Figure S2a). At a blending ratio of 0.6 (PF-DBT5/PFBT in weight), the PBdots exhibited a broad visible absorption band that extended to 600 nm and an efficient 650 nm emission with a quantum yield of 0.56 (Figure 1b, Figure S2b). This value represents the highest among various Pdots reported so far. The blending strategy was also successfully applied to other polymer donor–acceptor systems that consist of the light-harvesting polymer PFPV and different red-emitting polymers (Figure S3), thus indicating its general applicability for tuning of Pdot properties.

Chlorotoxin (CTX), a 36-amino acid peptide, was selected as a tumor-targeting ligand because it has a strong affinity for tumors of neuroectodermal origin.[28] We functionalized the PBdots by using an amphiphilic polymer, poly(styrene-co-maleic anhydride) (PSMA), to generate surface carboxyl groups (Figure 1a).[24] The carboxyl groups enabled CTX conjugation by standard carbodiimide chemistry.[29] Poly(ethylene glycol) (PEG) was also conjugated to reduce protein adsorption, limit immune recognition, and thereby increase the nanoparticle serum half-life in vivo. As a separate control, streptavidin was used to verify the conjugation strategy by specific cellular labeling. TEM indicated an average particle diameter of approximately 15 nm for the functionalized PBdots (Figure 1c). After conjugation to different molecules (PEG, CTX, and streptavidin), gel electrophoresis showed shifted migration bands of the PBdot conjugates in a 0.7% agarose gel, which is caused by the changes in surface charge and particle size (Figure 1d), thus indicating successful carboxyl functionalization and surface bioconjugation.

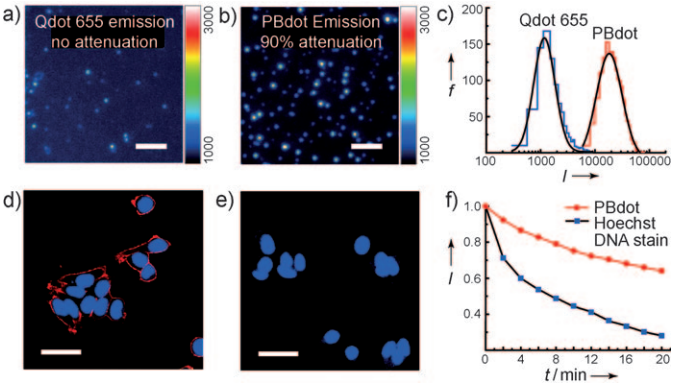

Figure 2. a) Single-particle image of Qdot 655. b) Single-particle image of PBdots. Scale bar, 4 μm. c) Intensity distributions of single-particle fluorescence. d) Confocal imaging of live MCF-7 cells incubated sequentially with anti-EpCAM primary antibody, biotinylated goat anti-mouse IgG secondary antibody, and PBdot-streptavidin conjugates. Red fluorescence was from PBdots and blue fluorescence was from the nuclear stain Hoechst 34580. Scale bar, 40 μm. e) Negative control for PBdot cell labeling (biotinylated secondary antibody was not used). f) Photobleaching curves extracted from confocal fluorescence images obtained under continuous laser scanning for 20 min.

We investigated the binding selectivity of PBdot bioconjugates. PBdot–streptavidin probes were used to label a specific cellular target, EpCAM, an epithelial cell-surface marker currently used for the detection of circulating tumor cells. Figure 2d shows that the PBdot–streptavidin successfully labeled EpCAM receptors on the surface of live MCF-7 human breast cancer cells after the cells were incubated sequentially with a primary anti-EpCAM antibody and a biotinylated goat antimouse immunoglobuline G (IgG)

secondary antibody. When the cells were incubated with primary antibodies and PBdot–streptavidin in the absence of the secondary antibody, fluorescence was not observed on the cell surface (Figure 2e), thus indicating that the PBdot bioconjugates were highly specific for the target. The photostability of PBdots was further compared to that of a small-molecule dye commonly used in cellular labeling. We monitored the fluorescence intensity changes of both the PBdot labeling of the cell surface and the Hoechst nuclear stain under continuous laser scanning for 20 minutes on a confocal microscope (Figure S5). Photobleaching curves extracted from the fluorescence images indicate that the PBdots were much more photostable than the organic dye (Figure 2f). The PBdots are also stable in serum for weeks, without aggregation and decrease in fluorescence intensity.

The delivery of imaging probes to brain tumors represents one of the most challenging in vivo tasks because of the exclusive blood–brain barrier and the complex dependence on the probe size and surface properties.[3] We evaluated the capability of the PBdot–CTX conjugate to traverse the blood–brain barrier and specifically target a tumor in a transgenic mouse model, ND2:SmoA1. We chose this mouse model because it closely resembles human medulloblastoma, the most common malignant childhood brain tumor.[30] The ND2:SmoA1 tumor arises spontaneously in the cerebellum and maintains an intact blood–brain barrier.[28] A detailed description of molecular targets of CTX for tumor targeting is provided in the Supporting Information. PBdot probes were injected into each animal, either symptomatic ND2:SmoA1 or wild type (as a control), through the tail vein. The PBdot probes were either targeting PBdot–CTX or nontargeting PBdot–PEG (as a probe control). The ability of PBdot probes to specifically target tumors was assessed by biophotonic imaging.

Figure 3a shows typical ex vivo biophotonic images of mouse brains at 72 hours post injection. Preferential accumulation of the PBdot–CTX in ND2:SmoA1 tumors was evident from the strong fluorescence signal observed only in the brain tumor regions of the mice that received the targeting probes (right image, middle row, Figure 3a). In contrast, significantly lower levels of fluorescence were detected in the tumors of mice that received the nontargeting PBdot–PEG probes (right image, top row, Figure 3a), hence indicating that the specific tumor targeting of PBdots is due to the conjugation with the CTX ligand. The ND2:SmoA1 mouse that did not receive an injection showed a similar fluorescence signal as those that received the nontargeting PBdot probes. Specific targeting of the PBdot–CTX probes to ND2:SmoA1 tumors was further counter-illustrated with wild-type mice (bearing no tumors) injected with the PBdot probes, which showed no PBdot accumulation in the healthy brains (Figure 3a, left). Comparable imaging results were obtained for ND2:SmoA1 and wild-type animals 24 hours after they were injected with PBdot probes (Figure S6), which suggest the accumulation of PBdot–CTX nanoprobe in the brain tumor was complete within 24 hours; the signal intensity remained steady for the remaining 48 hours of the 72-hour analysis.

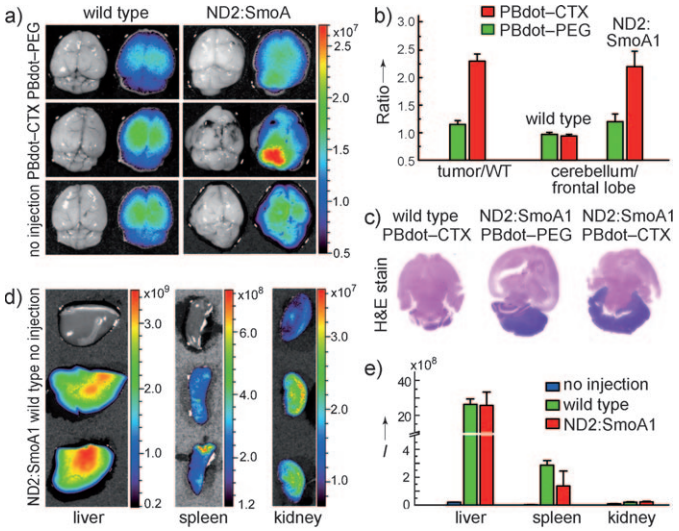

Figure 3. a) Fluorescence imaging of healthy brains in wild-type mice (left) and medulloblastoma tumors in ND2:SmoA1 mice (right). Each mouse was injected with either nontargeting PBdot–PEG (top), or targeting PBdot–CTX (middle); control: no injection (bottom). b) Tumor-targeting efficiency by quantifying fluorescence signals in ND2:SmoA1 versus wild-type mice and cerebellum versus frontal lobe. The biophotonic images (a) and (d) were acquired at 72 h post injection. The color gradient bar corresponds to the fluorescence intensity (p/s/cm^2/sr) of the images. c) Histological examination of the mouse brains in (a). d) Biophotonic images of resected livers, spleens, and kidneys from wild-type and ND2:SmoA1 mice receiving Pbdot-CTX injection. e) Biodistribution of the PBdot probes in the resected organs. Each data point in (b) and (e) is the (mean ± standard deviation) from $n = 3$ animals.

Quantitative evaluation of the PBdot accumulation further confirmed the specific tumor targeting of the PBdot–CTX conjugates. When the targeting PBdot–CTX probes were injected, the fluorescence intensity in the brain regions of ND2:SmoA1 relative to wild-type animals showed a (2.3 ± 0.2)-fold increase ((mean ± standard deviation), $P < 0.01$), compared with a minimal change ($(1.2 \pm 0.1$ fold), $P > 0.05$) when using nontargeting PBdot–PEG probes (Figure 3b). This signal increase was comparable to the NIR-emitting CTX:Cy5.5 bioconjugate.[28] For a given ND2:SmoA1 or wild-type animal, fluorescence intensity in the frontal lobe (healthy tissue) of the cerebral hemisphere and the cerebellum (tumor-containing tissue) in the same animal was also analyzed (Figure 3b). Again, significant signal increase ((2.2 ± 0.3)-fold, $P < 0.01$) in the cerebellum versus the frontal lobe was only observed in the ND2:SmoA1 mice that received targeting PBdot–CTX probes, whereas a minimal change ((1.1 ± 0.2)-fold, $P > 0.05$) was seen for the ND2:SmoA1 mice that received nontargeting PBdot–PEG probes. No apparent difference in signal between the cerebellum and the frontal lobe was observed in wild-type animals regardless of whether targeting or nontargeting probes were injected. To determine the accuracy of tumor regions as highlighted by PBdot–CTX, histological analysis was performed on the excised brains of the mice after biophotonic imaging. The dark purple regions in the hematoxylin and eosin(H&E)-stained cerebellum of the

ND2:SmoA1 mice clearly outline the tumors as compared to the wild-type mouse (Figure 3c). The histological analysis correlated well with the biophotonic images and confirmed the selective accumulation of the targeting PBdot–CTX probes in the malignant brain tumors.

The nanoparticle clearance and biodistribution are closely dependent on particle size.[31,32] For nanoparticles that have a hydrodynamic diameter of 10–20 nm, the only major route of excretion from the animal body is through the liver into bile and feces.[32] There was no observable fluorescence signal in the blood at 72 hours post injection of the PBdot–CTX probes (Figure S7). We investigated the distribution profiles in the main clearance organs including liver, spleen, and kidney by ex vivo fluorescence signal quantification of the resected tissues (Figure 3d). The biodistributions in the wild-type animals that received the PBdot–CTX injection and the ND2:SmoA1 mice that were not injected were also analyzed (Figure 3d). As expected based on particle size,[32] the PBdot–CTX exhibited dominant uptake in the liver, a significantly lower signal in spleen, and nearly no distribution in the kidney for both wild-type and ND2:SmoA1 mice (Figure 3e). This distribution profile is comparable to those reported for inorganic iron oxide nanoparticles and quantum dots of similar particle size.[3,32]

In summary, we designed a polymer-blend nanodot system that consists of donor–acceptor polymers for in vivo tumor targeting. The large absorptivity and high fluorescence quantum yield make the PBdots approximately 15 times brighter than the Qdots that emit at 655 nm. To the best of our knowledge, the PBdots represent the brightest nanoprobe at present among various fluorescent nanoparticles of similar size (ca. 15 nm). We covalently conjugated the PBdots to a peptide ligand CTX, and demonstrated their specific targeting to malignant brain tumors by biophotonic imaging, biodistribution, and histological analyses. This study provides a new type of nanoparticle platform that holds promise for clinical cancer diagnostics.

Experimental Section

Functionalized PBdots in aqueous solution were prepared by using a modified nanoprecipitation method. Surface bioconjugation was performed by utilizing the EDC-catalyzed reaction between carboxyl PBdots and the respective amine-containing biomolecules.

All mouse studies were conducted with procedures approved by the Institutional Animal Care and Use Committee at Fred Hutchinson Cancer Research Center. Transgenic ND2:SmoA1 mice were generated on a C57BL/6 background. Nongenetically altered C57BL/6 mice were used as wild-type controls. ND2:SmoA1 mice or C57BL/6 wild-type controls were injected with PBdot–CTX or PBdot–PEG (50 μL; 1 μM solution) through the tail vein. One or three days after injection, the mice were euthanized by using CO_2 inhalation and their brains were removed for ex vivo fluorescent imaging. Ex vivo images were obtained by using the Xenogen/Caliper Spectrum Imaging System. For biodistribution, C57BL/6 wild-type and ND2:SmoA1 mice were injected with PBdot–CTX (50 μL; 1 μM) through the tail vein. Three days after injection, the mice were euthanized, blood, liver, kidney, and spleen were removed and analyzed using ex vivo imaging techniques as described above. A full description of the materials and methods are provided in the Supporting Information.

Received: November 28, 2010
Revised: February 7, 2011
Published online: March 4, 2011

Keywords: fluorescence · imaging agents · nanoparticles · semiconducting polymers · tumors

[1] M. Ferrari, *Nat. Rev. Cancer* **2005**, *5*, 161.
[2] S. Sengupta, D. Eavarone, I. Capila, G. L. Zhao, N. Watson, T. Kiziltepe, R. Sasisekharan, *Nature* **2005**, *436*, 568.
[3] O. Veiseh, C. Sun, C. Fang, N. Bhattarai, J. Gunn, F. Kievit, K. Du, B. Pullar, D. Lee, R. G. Ellenbogen, J. Olson, M. Q. Zhang, *Cancer Res.* **2009**, *69*, 6200.
[4] R. Popovtzer, A. Agrawal, N. A. Kotov, A. Popovtzer, J. Balter, T. E. Carey, R. Kopelman, *Nano Lett.* **2008**, *8*, 4593.
[5] X. Gao, Y. Cui, R. M. Levenson, L. W. K. Chung, S. Nie, *Nat. Biotechnol.* **2004**, *22*, 969.
[6] I. L. Medintz, H. T. Uyeda, E. R. Goldman, H. Mattoussi, *Nat. Mater.* **2005**, *4*, 435.
[7] X. Michalet, F. F. Pinaud, L. A. Bentolila, J. M. Tsay, S. Doose, J. J. Li, G. Sundaresan, A. M. Wu, S. S. Gambhir, S. Weiss, *Science* **2005**, *307*, 538.
[8] A. M. Derfus, W. C. W. Chan, S. N. Bhatia, *Nano Lett.* **2004**, *4*, 11.
[9] C. Wu, C. Szymanski, J. McNeill, *Langmuir* **2006**, *22*, 2956.
[10] C. Wu, C. Szymanski, Z. Cain, J. McNeill, *J. Am. Chem. Soc.* **2007**, *129*, 12904.
[11] C. Wu, B. Bull, C. Szymanski, K. Christensen, J. McNeill, *ACS Nano* **2008**, *2*, 2415 – 2423.
[12] J. Pecher, S. Mecking, *Chem. Rev.* **2010**, *110*, 6260.
[13] A. Kaeser, A. P. H. J. Schenning, *Adv. Mater.* **2010**, *22*, 2985.
[14] J. H. Moon, W. McDaniel, P. MacLean, L. E. Hancock, *Angew. Chem.* **2007**, *119*, 8371; *Angew. Chem. Int. Ed.* **2007**, *46*, 8223.
[15] K. Y. Pu, K. Li, J. B. Shi, B. Liu, *Chem. Mater.* **2009**, *21*, 3816.
[16] R. Abbel, R. van der Weegen, E. W. Meijer, A. P. H. J. Schenning, *Chem. Commun.* **2009**, 1697.
[17] M. C. Baier, J. Huber, S. Mecking, *J. Am. Chem. Soc.* **2009**, *131*, 14267 – 14273.
[18] P. Howes, M. Green, J. Levitt, K. Suhling, M. Hughes, *J. Am. Chem. Soc.* **2010**, *132*, 3989 – 3996.
[19] C. Wu, Y. Zheng, C. Szymanski, J. McNeill, *J. Phys. Chem. C* **2008**, *112*, 1772.
[20] C. Wu, B. Bull, C. Szymanski, K. Christensen, J. McNeill, *Angew. Chem.* **2009**, *121*, 2779 – 2783; *Angew. Chem. Int. Ed.* **2009**, *48*, 2741 – 2745.
[21] P. Howes, M. Green, A. Bowers, D. Parker, G. Varma, M. Kallumadil, M. Hughes, A. Warley, A. Brain, R. Botnar, *J. Am. Chem. Soc.* **2010**, *132*, 9833.
[22] S. Kim, C. K. Lim, J. Na, Y. D. Lee, K. Kim, K. Choi, J. F. Leary, I. C. Kwon, *Chem. Commun.* **2010**, *46*, 1617.
[23] C. Wu, T. Schneider, M. Zeigler, J. Yu, P. Schiro, D. Burnham, J. D. McNeill, D. T. Chiu, *J. Am. Chem. Soc.* **2010**, *132*, 15410.
[24] C. Wu, Y. Jin, T. Schneider, D. R. Burnham, P. B. Smith, D. T. Chiu, *Angew. Chem.* **2010**, *122*, 9626; *Angew. Chem. Int. Ed.* **2010**, *49*, 9436.
[25] Q. Hou, Q. M. Zhou, Y. Zhang, W. Yang, R. Q. Yang, Y. Cao, *Macromolecules* **2004**, *37*, 6299.
[26] R. Q. Yang, R. Y. Tian, J. G. Yan, Y. Zhang, J. Yang, Q. Hou, W. Yang, C. Zhang, Y. Cao, *Macromolecules* **2005**, *38*, 244.
[27] C. Wu, H. Peng, Y. Jiang, J. McNeill, *J. Phys. Chem. B* **2006**, *110*, 14148.
[28] M. Veiseh, P. Gabikian, S. B. Bahrami, O. Veiseh, M. Zhang, R. C. Hackman, A. C. Ravanpay, M. R. Stroud, Y. Kusuma, S. J.

Hansen, D. Kwok, N. M. Munoz, R. W. Sze, W. M. Grady, N. M. Greenberg, R. G. Ellenbogen, J. M. Olson, *Cancer Res.* **2007**, *67*, 6882.
[29] G. T. Hermanson, *Bioconjugate Techniques*, 2nd ed., Academic Press, San Diego, **2008**.
[30] B. A. Hatton, E. H. Villavicencio, K. D. Tsuchiya, J. I. Pritchard, S. Ditzler, B. Pullar, S. Hansen, S. E. Knoblaugh, D. Lee, C. G. Eberhart, A. R. Hallahan, J. M. Olson, *Cancer Res.* **2008**, *68*, 1768.
[31] H. S. Choi, W. H. Liu, F. B. Liu, K. Nasr, P. Misra, M. G. Bawendi, J. V. Frangioni, *Nat. Nanotechnol.* **2010**, *5*, 42.
[32] H. S. Choi, W. Liu, P. Misra, E. Tanaka, J. P. Zimmer, B. I. Ipe, M. G. Bawendi, J. V. Frangioni, *Nat. Biotechnol.* **2007**, *25*, 1165.

